THE JOURNAL OF PHYSICAL CHEMISTRY C
A JOURNAL OF THE AMERICAN CHEMICAL SOCIETY

pubs.acs.org/JPCC

Article

Atomic-Scale STEM Analysis Shows Structural Changes of Au–Pd Nanoparticles in Various Gaseous Environments

Published as part of The Journal of Physical Chemistry virtual special issue "Cynthia Friend Festschrift".

Alexandre C. Foucher, Cameron J. Owen, Tanya Shirman, Joanna Aizenberg, Boris Kozinsky, and Eric A. Stach*

Cite This: *J. Phys. Chem. C* 2022, 126, 18047–18056

Read Online

ACCESS | Metrics & More | Article Recommendations | Supporting Information

ABSTRACT: We report dynamical restructuring effects in free-standing $Au_{0.75}Pd_{0.25}$ nanoparticles occurring in gaseous environments at elevated temperatures. The freshly prepared sample was found to have a core–shell structure with a Pd-rich phase on the surface. The evolution of sample composition and morphology under exposure to 1 bar of pure gases, namely O_2, H_2, air, CO, and CO_2, at different temperatures was studied using *in situ* scanning transmission electron microscopy (STEM) and energy-dispersive X-ray spectroscopy (EDS). We observed sharper facets on the surface of the particles under O_2 or air at 400 °C. Small islands of Pd were present on the surface, although some Pd was redistributed inside the bulk when the temperature was increased under O_2. Subtle changes in surface roughness were noted when O_2 was substituted with H_2 at 400 °C, an observation correlated to density functional theory (DFT) calculations. The particles lost clean surface facets when CO was introduced at room temperature and at 200 °C. No substantial changes could be observed after exposure to CO_2 at 250 °C. The adsorption of CO molecules on the surface modifies the surface of the particles and decreases the facet prevalence. These *in situ* observations show how gases can induce subtle modification of the surface of nanocatalysts, potentially impacting their chemical properties.

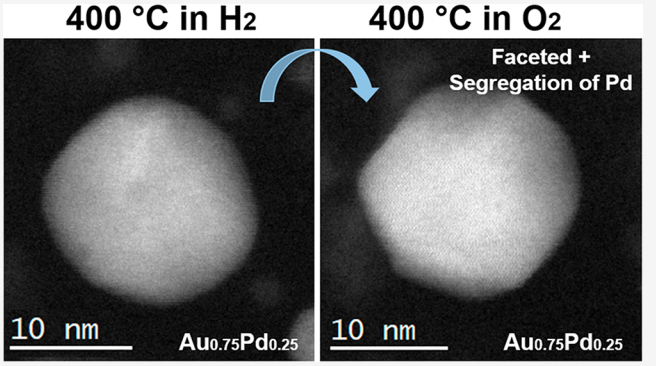

INTRODUCTION

Pd is an excellent catalyst used for a large range of reactions, such as CO oxidation,[1,2] reduction of NO,[3] and hydrogenation of alkynes into alkenes.[4−7] However, Pd is an expensive transition metal that is not always highly selective.[7−9] Nevertheless, it has been shown that chemical properties of Pd can be tuned by alloying it with another transition metal.[10,11]

One advantageous combination is the alloying of Pd with Au: Often, Pd is diluted in Au to optimize the use of Pd and enhance its catalytic properties.[12] For instance, Au–Pd alloys have been used for the hydrogenation of butadiene and outperformed the monometallic counterparts.[13] In other cases, they have been used for the hydrogen exchange reaction, where the alloy phase leads to strong activity.[14] Recent studies have also focused on the electrocatalytic properties of Au–Pd systems to reduce CO_2 to a mixture of C1–C5 hydrocarbons.[15] This reactivity is associated with the reaction of adsorbed CO and $-CH_2$ intermediates on the surface, which ultimately led to the formation of longer hydrocarbons. Au–Pd alloys can be created to optimize the use of Pd by keeping Pd atoms well distributed on the surface,[13,14] but this preference has not been studied extensively.[16,17]

These examples show how Au–Pd nanostructures can be used in the field of catalysis. However, their catalytic properties are strongly dependent upon particle structure. It is known that composition, oxidation state, and morphology are crucial parameters for tuning catalytic activity. In particular, the surface structure and the configuration of facets strongly affect catalytic properties.[18−20] Pure Au particles have been extensively investigated with *in situ* methods, which have shown changes in facet orientations and surface roughness upon exposure to gaseous environments at elevated temperatures.[21−23] However, Au–Pd systems have been the subject of very few *in situ* studies. The impact of Pd insertion in a gold crystal is not well understood, especially under different gases

Received: August 18, 2022
Revised: September 19, 2022
Published: October 14, 2022

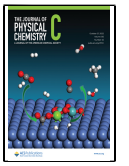

and temperatures. Furthermore, influence of Pd oxidation in Au−Pd systems is not well described and could be crucial in the morphological changes. In fact, modification of surface structure such as facet reconstruction can cause changes in adsorption and desorption energies and ultimately impact the catalytic properties.[24,25] Additionally, migration of Pd and Au atoms within the particles in realistic catalytic reaction conditions can cause decreased catalytic activity and selectivity.[26,27]

To address these questions, we performed atomic-scale *in situ* STEM analysis of free-standing Au−Pd particles in gaseous atmospheres (O_2, H_2, CO, or CO_2) at different temperatures. Results were correlated to DFT calculations of the surface energy of Pd and the Au−Pd surface to explain the underlying thermodynamic preference for morphological change observed during the experiments.

MATERIALS AND METHODS

Experiment. $Au_{0.75}Pd_{0.25}$ particles were prepared following a previously published procedure.[28] For *in situ* STEM measurements of a sample of free-standing particles, a custom-made cell with SiN windows was used. We chose to study an Au−Pd sample with a concentration of 25% of Pd for two reasons: It is low enough to be considered a representative sample of Au−Pd catalyst with dilute Pd but high enough to obtain excellent EDS and EELS data, which are critical in this study. *Ex situ* and *in situ* analyses (at 1 bar of gas) were performed with a JEOL NEOARM operating at 200 kV. The $Au_{0.75}Pd_{0.25}$ particle samples were sandwiched between the two windows and inserted in a dedicated environmental TEM holder manufactured by Hummingbird Scientific.[29,30] The cell contained a microcoil for temperature control and two inlets allowing gases to flow into the cell. Control of the flow was achieved with a gas delivery system manufactured by Hummingbird Scientific. All data were collected under a gaseous atmosphere at the indicated temperatures. Only ultrahigh-purity (UHP) gases were used, with a flow of 5 sccm. Energy-dispersive X-ray spectroscopy (EDS) maps and electron energy-loss spectroscopy (EELS) were performed to determine compositional heterogeneities with particles as well as the oxidation state of Pd. For imaging, the camera length used with the JEOL NEOARM was 4 cm, with a probe current of 500 pA. For EDS and EELS, the camera length was 2 cm and the probe current was 700 pA. For low pressure *in situ* analysis, an environmental TEM (Hitachi HF5000) was used.

Two sets of experiments of particle treatment with different gases at different temperatures were performed, as summarized in Figure 1. The gases and temperature ranges were chosen to reflect common environmental conditions for Au−Pd samples used as a catalysts.[7,12] In the first set, the temperature was increased at 10 °C/min to 400 °C under 1 bar of O_2. Exposure to O_2 at elevated temperatures removed all ligands and carbon contamination. The sample was kept under these conditions for 2 h. The cell was then purged with N_2, after which H_2 was introduced at 400 °C for 1 h. Then, the cell was purged again with N_2 and filled with O_2. The temperature was decreased to 250 °C under O_2, the cell was purged with N_2, and then CO_2 was provided for 1 h. The second set is similar to the first one, except for the last step: The temperature was decreased under O_2 to 200 °C, before the cell was purged with N_2, and then filled with CO for 1 h. CO treatment after the CO_2 experiment was avoided, as we wanted to compare CO and CO_2 exposures after oxidation. Furthermore, this ensures that structural

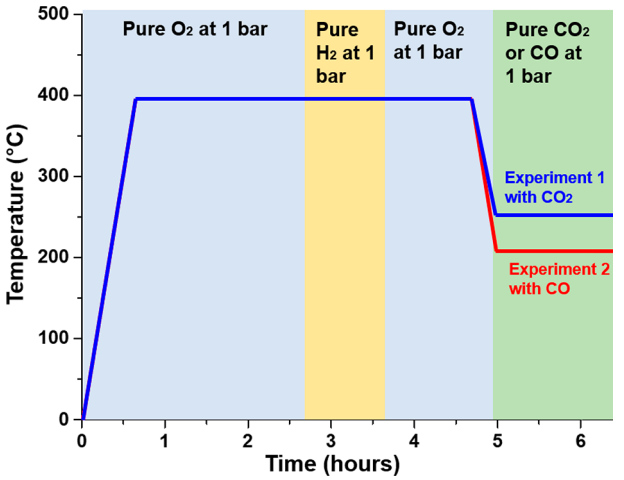

Figure 1. Summary of conditions used for the two sets of experiments performed on free-standing $Au_{0.75}Pd_{0.25}$ particles. Experiments 1 and 2 are identical, except for the last step. In the first case, CO_2 was used at 250 °C. In the second experiment, CO was used at 200 °C. Only pure gases were used at 1 bar.

modifications from CO_2 or CO were not resulting from an initial treatment with either CO_2 or CO.

DFT Calculations. All calculations performed in this study were completed using the Vienna Ab initio Simulation Package (VASP).[31] The Perdew−Burke−Ernzerhof (PBE) exchange-correlation functional in the Projector-Augmented Wave (PAW) formalism was employed for all elements.[32,33] The pseudopotentials chosen for Au, Pd, and O did not include any semicore corrections. The cutoff energy was set to 450 eV, and the *k*-point grids were optimized for each system (such that total energies were <5 meV/atom). Methfessel−Paxton smearing of the electron density at the Fermi level was employed, using a smearing value of 0.2 eV, as is typical for metallic systems. All calculations were spin-polarized, which is necessary to capture the correct electronic ground state of O_2 (spin triplet).

Surface free energies were computed for each system using bulk references and gas-phase O_2 when permitted. Explicitly, the surface energies are calculated via eq 1:

$$G_{\mathrm{surf,form}} = \frac{E_{\mathrm{total}} - i(E_{\mathrm{Au}}) - j(E_{\mathrm{Pd}}) - \frac{k}{2}(E_{\mathrm{O_2}})}{2A_{\mathrm{surf}}} \quad (1)$$

where E_{total} represents the total energy of the system, i is the number of Au atoms in the total system, E_{Au} is the energy per atom of Au in the bulk, j is the number of Pd atoms in the total system, E_{Pd} is the energy per atom of Pd in the bulk, k is the number of O atoms in the total system, $E_{\mathrm{O_2}}$ is the corrected and entropy corrected value for one O_2 molecule in the gas phase (both corrections are discussed below), and A_{surf} is the surface area of one side of the system. Because of the overbinding of oxygen, as was characterized previously,[34] we correct the oxide energies by +0.53 eV per oxygen molecule, which represents the energy difference between the PBE-predicted bond energy of O_2 and the experimental dissociation energy.

Hence, the energy "zero" represents the relevant bulk Au, bulk Pd, and gaseous O_2 contributions to whichever surface is considered, in which the mass balance is inherent. Lastly, we include entropic contributions to the surface free energy of

https://doi.org/10.1021/acs.jpcc.2c05929
J. Phys. Chem. C 2022, 126, 18047−18056

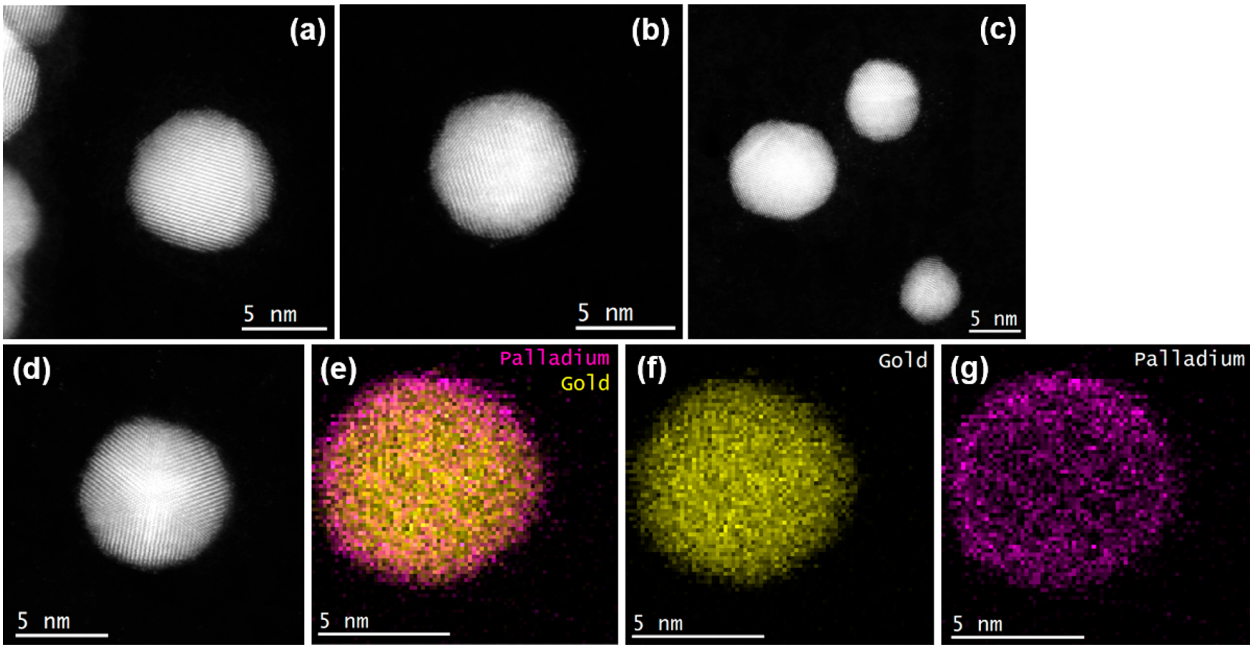

Figure 2. (a–c) Representative HAADF-STEM images of free-standing $Au_{0.75}Pd_{0.25}$ particles. It is possible to distinguish dimmer brightness at the edges of the particles. This is due to the increased concentration of Pd on the surface, which has a lower atomic number than Au. (d–g) HAADF-STEM image and EDS maps of $Au_{0.75}Pd_{0.25}$ particles. (d) HAADF-STEM image of the particle analyzed with EDS. (e) Combined Pd and Au EDS maps showing the increased concentration of Pd on the edges. (f) Au EDS map. (g) Pd EDS map.

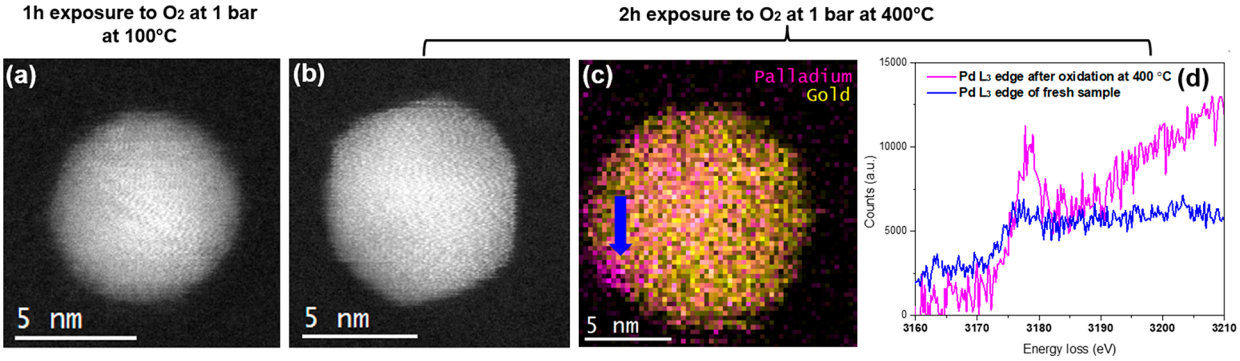

Figure 3. STEM-EDS/EELS analysis of the particles exposed to an O_2-rich environment. P_{O_2} is 1 bar. (a, b) Analysis of a particle after heating under O_2 at 100 °C. The facets are sharper at higher temperature. Hence, heating under O_2 affects the surface roughness of $Au_{0.75}Pd_{0.25}$ particles. (c, d) STEM-EDS analysis after 2 h exposure to O_2 at 400 °C. (c) EDS map of another particle, with segregation of Pd on the edges shown by the blue arrow. No core–shell configuration is visible, on either the images or the EDS map. Also, we used an above-average size particle to minimize potential beam-induced effects. (d) EELS spectra from the Pd edge after 2 h of O_2 exposure (magenta line). The increase of the peak (called white line) in the Pd near edge region indicates oxidation after the treatment.

each oxide material. This is accomplished using the Atomic Simulation Environment's Thermochemistry package where the experimental conditions are included in the total energy of each O_2 molecule.[35]

RESULTS

First, *ex situ* STEM analysis was performed to determine the characteristics of freshly synthesized $Au_{0.75}Pd_{0.25}$ particles. These analyses were completed for the specific times indicated, as displayed in Figure 1. STEM imaging was performed at high magnification, and EDS maps were collected. These data are summarized in Figure 2 and indicate a core–shell configuration with Pd primarily on the surface of the particle. This is also observed from high-angle annular dark-field (HAADF) STEM images, where the particle brightness is substantially less intense on the edges. This dimer shell cannot be attributed to a thickness effect, and previous studies have shown that the brightness in HAADF-STEM is proportional to $Z^{1.65}$.[36] Hence, because Z_{Pd} = 46 and Z_{Au} = 79, it is possible to see Pd segregation on STEM images. This result is also confirmed with EDS maps, clearly showing a core–shell configuration with a Pd-rich layer on the surface with a thickness smaller than 1 nm. Additional EDS maps from more particles are shown in Figure S1, indicating that the core–shell configuration is present for most particles in the sample. This core–shell configuration is due to the synthesis process, as Au nanoparticles nucleate before the addition of Pd precursors.[28] During the synthesis, Pd will coalesce on the nucleated Au particles and form a Pd shell, so the core–shell configuration is due to a kinetic effect. This has been observed in another publication about Au–Pd samples.[27]

https://doi.org/10.1021/acs.jpcc.2c05929
J. Phys. Chem. C 2022, 126, 18047–18056

An EELS spectrum from the Pd L_3 edge at 3173 eV was also collected, and it indicated partial oxidation of Pd in the system, as shown in Figure 3. Indeed, a typical "white line" consistent with the presence of PdO can be seen.[37] For metallic Pd, no white line is present.[38] This spectral feature arises from energy transitions in PdO between the 1s orbital and the 4d orbital, which are not present in metallic Pd. The peak is not as prominent as would be expected for a pure PdO phase, which leads us to believe that Pd is only partially oxidized in the sample. Reference signals for Pd and PdO in a previous study clearly support this hypothesis.[38] We also detected the presence of O in the $Au_{0.75}Pd_{0.25}$ particles, with the O K edge at 529 eV (Figure S2), confirming the presence of PdO in the structure. No signal for O was obtained in surveyed regions without $Au_{0.75}Pd_{0.25}$ particles. Finally, it should be noticed that a minority of particles have an icosahedral shape, which is typically found in small Au particles.[39]

After *ex situ* analysis, the free-standing sample was deposited into the gas cell for *in situ* STEM analysis. The sample was exposed to pure O_2 at room temperature (RT), and the temperature was increased at a rate of 10 °C/min to 400 °C. Figure 3 shows a set of STEM images as well as EDS and EELS data taken after 2 h of exposure to O_2 at 400 °C at a pressure of 1 bar. *In situ* microscopy with atomic resolution at high pressure (≥1 bar) was achieved. The exposure to elevated temperatures leads to the disruption of the core−shell structure, with migration of Pd from the shell to the Au-rich core. This is commonly seen in core−shell structures.[13,40,41] The particles appear highly faceted, and the edges are sharper compared to the *ex situ* STEM observations at room temperature. A statistical analysis is provided in Table S1 to show how many particles changed after oxidation. All particles showed a change in morphology with the formation of sharp and distinctive facets after oxidation of the fresh particles. In Figure 3a,b, two images of the same particle were taken when the temperature was increased. At 100 °C, the particles still had edges with some roughness. At 400 °C, the surface roughness is diminished; the facets are straight and are clearly visible. To remove interference from residual carbon species coming from the solvents used, a careful plasma cleaning of the chip with sample was performed, and measurements were performed at 100 °C rather than room temperature.

A significant minority of $Au_{0.75}Pd_{0.25}$ particles had an icosahedral shape after O_2 treatment for 2 h at 400 °C (Figure S3). Interestingly, EDS maps of the particles showed that Pd-rich islands are present on the edges of the particles (Figure 3c). Additional EDS maps after O_2 treatment presented in Figure S4 indicate a general trend where small Pd-rich islands formed on the surface of the particles.[42] The core−shell configuration seemingly no longer exists, and the relatively thick Pd-rich shell is not present. Instead, small Pd islands are distinguishable on the edges, and the depth is estimated to be <5 atomic monolayers on average. Overall, we conclude that some Pd redistribution occurred during *in situ* heating under O_2. Analysis of the same particle when the temperature was slowly increased and after long exposure to O_2 at 400 °C also indicates a thick Pd-rich region (Figure S5). We used the same pixel size and pixel time for the two maps and selected larger-than-average particles to limit beam-induced effects. After long exposure to O_2 at 400 °C, the shell is no longer visible (with the same STEM parameters).

Finally, EELS analysis of the Pd L_3 edge at 3173 eV was performed on many particles and compared to the EELS spectrum collected for the *ex situ* STEM analysis (Figure 3d). To this end, post-specimen lenses were manually adjusted to optimize the signal-to-noise ratio and detect changes in the valence state of Pd. The spectra were collected over 30−40 particles. EELS indicated an increase in the oxidation level of Pd after the O_2 treatment. In fact, a peak (called "white line") is detected for the Pd L_3 edge after oxidation. This white line is a signature for PdO, as described above. Additionally, a small shift to higher energy losses is observed when Pd is oxidized, which is what is expected. Oxidized Pd has fewer electrons than metallic Pd, so the remaining electrons are more pulled to the core of the atoms by the protons. Hence, additional energy is needed to perform energy transitions, and ultimately, higher energy losses occur for the transmitted electron of the beam.

After O_2 treatment, the cell was purged with nitrogen; H_2 was introduced at the same temperature (400 °C), and the sample was exposed to these conditions for 1 h. Figure 4 shows

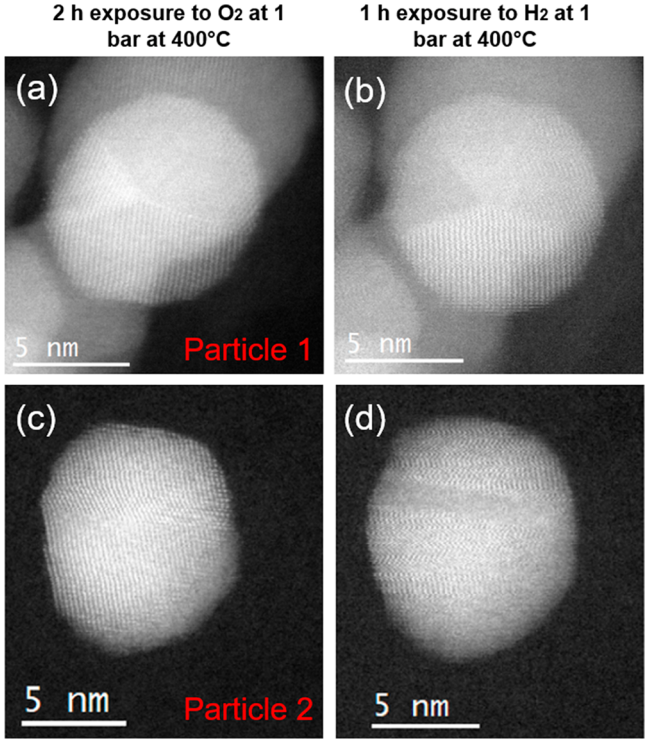

Figure 4. *In situ* HAADF-STEM images of $Au_{0.75}Pd_{0.25}$ particles after O_2 and H_2 exposure at 400 °C under 1 bar. (a, b) Representative image of a majority of particles. No obvious change of the surface roughness was observed. A slight modification of the morphology is observed as the particle is more spherical after H_2 treatment. The facets did not seem to undergo a major transformation, and the particle retained an icosahedral shape. (c, d) Image of a second particle undergoing restructuring at the surface after exposure to H_2. The surface is rougher, and sharp edges are more difficult to distinguish than after O_2 exposure. The same microscopy parameters were used, and the Ronchigram was adjusted before imaging to obtain the best imaging quality possible. The focus was adjusted to avoid blurriness, and in both cases, atomic resolution was achieved.

in situ atomic-resolution STEM images of the surface of $Au_{0.75}Pd_{0.25}$ particles. For the large majority of particles, the surface remained unchanged after H_2 was introduced. However, in some cases, the edge of the particles appeared rougher, as shown in Figure 4c,d. A statistical analysis is provided in Table S1. Only images with very high

https://doi.org/10.1021/acs.jpcc.2c05929
J. Phys. Chem. C 2022, 126, 18047−18056

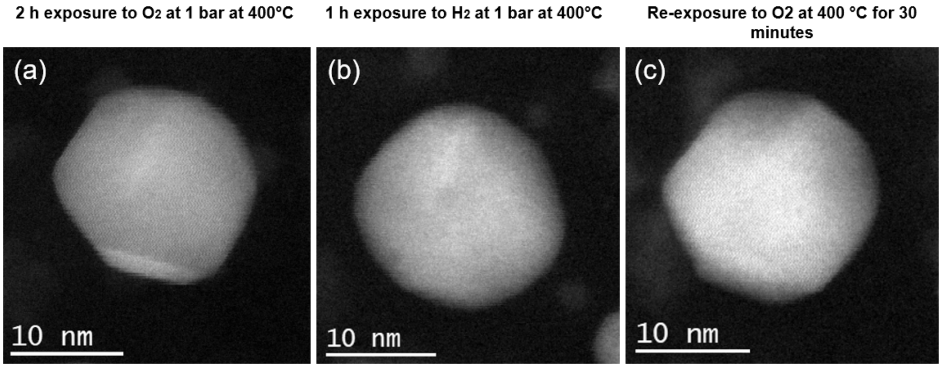

Figure 5. An example of a reversible change in the morphology during an oxidation−reduction−oxidation cycle. The pressure of gases is 1 bar. (a) Particle after oxidation at 400 °C for 2 h. (b) Particle after reduction at 400 °C for 1 h. (c) Particle after reoxidation at 400 °C for 30 min. The sharp edges and the corners visible after the first oxidation reappear upon reoxidation. The oxidation of Pd seems to play a role in the surface structure of the $Au_{0.75}Pd_{0.25}$ particles. We chose a particle with above-average size during this analysis to minimize beam-induced effects. Smaller particles are more sensitive to the electron beam than larger particles.

magnification and resolution were considered for this statistical analysis. We showed that 2/3 of the particles remained unchanged upon reduction, whereas 1/3 of the particles showed some slight change in surface roughness. It should be emphasized that the particles were exposed to the electron beam only during imaging. Furthermore, when STEM images were not being actively collected, the beam valve was closed to avoid beam-induced effects. Hence, we believe that the subtle changes in the surfaces of the particles upon exposure to H_2 after oxidation under O_2 are the results of a change in the environment. In some cases, changes in the edges were reversible, as shown in Figure 5. Re-exposure to O_2 at 400 °C followed the reduction with H_2 at 400 °C. During this re-exposure, most particles that changed upon H_2 exposure recovered a highly faceted morphology (observed after first O_2 treatment) upon reoxidation (second O_2 treatment).

It should be noted that no Pd islands were observed in particles after exposure to H_2 at elevated temperatures. Previous studies of Au−Pd materials showed redistribution of Pd atoms within the particles, as there was no driving force for the formation of Pd oxide on the surface.[16] EDS maps confirmed the uniform distribution of Pd within particles, with no segregation of Pd on the surface (Figure S6). Additional STEM images are provided in Figures S7 and S8 to show statistics with a bigger sample size about the shape of the particles upon redox cycling. Indexing of facets of particles after exposure to O_2 treatment was also performed in Figure S9 and showed a high number of (111) facets. Additionally, the experiment was also performed with low pressures of O_2 or H_2 (5×10^{-2} Pa) with an environmental TEM. Similar changes were observed in the particles as those observed at 1 bar. Exposure to 5×10^{-2} Pa of O_2 also led to the formation of sharp facets, and exposure to 5×10^{-2} Pa of H_2 caused a slight increase in surface roughness in some particles (Figure S10). Hence, we conclude that morphology changes can also occur at low pressures of gases and are not only valid for high-pressure conditions.

Finally, the experiment was finished with exposure of the system to CO_2 at 250 °C. We did not observe facet reconstruction. Because we can clearly distinguish the facets with *in situ* measurements, we concluded that no reconstruction happened (see also Table S1). Additional STEM images are provided in Figure S11. This is hypothesized as the inability of Pd or Au to interact with CO_2 molecule as no CO_2 reduction is observed under 1 atm at temperatures ranging from 25 to 250 °C. Previous analyses are also suggesting the weak interaction between Pd and CO_2 molecules.[43,44] Additionally, one can hypothesize that Au passivates Pd by making interaction between Pd and CO_2 molecules less energetically favorable. Differences between the O_2 treatment at 400 °C and the exposure to CO_2 at room temperature are shown in Figure 6. An additional EDS map is also provided in Figure S12.

After experiment 1 with CO_2 exposure, experiment 2 was performed, with the same redox cycle at the beginning, but with exposure to CO at 200 °C instead of using CO_2 at 250 °C. These results are summarized in Figure 7, where drastically different dynamics are observed compared to the CO_2 experiment. The particles appeared to be less faceted and were more sensitive to beam exposure. The loss of facets has been observed in all particles (Table S1). The particle morphology changes occurred quickly after exposure to CO. This is due to the strong interaction between Pd and CO.[45] It has also been shown that adsorption of CO on under-coordinated Pd leads to surface roughening.[46] Another factor to consider is the induced surface stress to the facets upon CO adsorption.[47,48] This causes facet reconstruction, visible in the images provided in Figure 7. Changes in morphology are not due to redistribution of Pd atoms within the particles: Figure 7d indicates no preferential segregation of Pd after exposure to CO at elevated temperature.

It should be stressed that metal deposition on the sample was not detected during the CO treatment. Indeed, deposition of carbon monoxide−metal complexes during *in situ* experiments is frequent, as CO molecules are bonded to metallic compounds in the *in situ* setup and are then deposited on the sample. Interaction between the metal carbonyls and sample could potentially lead to incorrect conclusions.[49] The *in situ* setup employed here is made of stainless steel, but no Fe was detected with EDS or EELS (see Figure S13). Additional STEM images of particles before and after CO treatment are also provided in Figures S14 and S15 to show that the surface roughening is substantial on a majority of particles. Some facet reconstruction could also be observed in Figure S16.

To better understand the role of Pd and PdO in facet reconstruction, the surface energies of different Pd and Au−Pd surfaces were calculated. To simplify the calculations, the effect of twin boundaries and grain boundaries was not factored in as

https://doi.org/10.1021/acs.jpcc.2c05929
J. Phys. Chem. C 2022, 126, 18047−18056

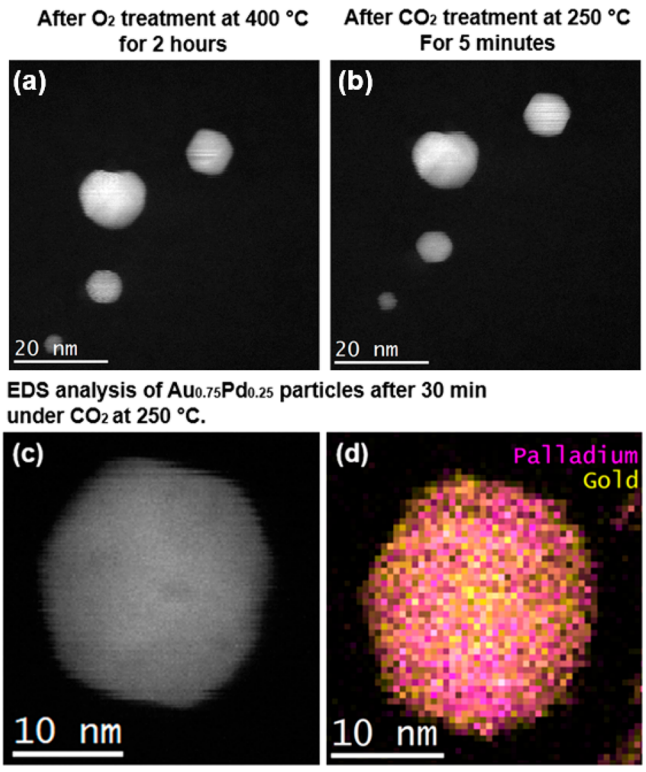

Figure 6. STEM-EDS analysis of the effect of 1 bar of CO_2 on the structure of $Au_{0.75}Pd_{0.25}$. (a, b) HAADF STEM analysis before and after exposure to CO_2. In (b), the particles appear rounder, and sharp facets are less present. (c, d) STEM EDS analysis of a particle after 30 min under CO_2 at 250 °C. No preferential segregation of Pd was observed. On the basis of quantification with EDS, this specific particle had a slightly higher Pd concentration due to heterogeneities in the sample.

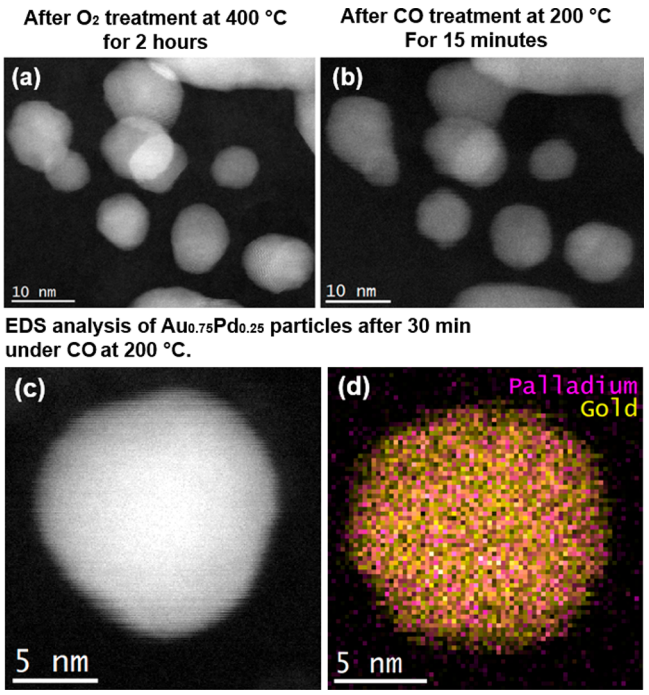

Figure 7. STEM-EDS analysis of the effect of 1 bar of CO on the structure of $Au_{0.75}Pd_{0.25}$. (a, b) HAADF STEM analysis before and after exposure to CO. In (b), sharp facets are less present. The surface of the particles appears more irregular than after the O_2 treatment. (c, d) STEM EDS analysis of a particle after 30 min under CO_2 at 250 °C. No preferential segregation of Pd was observed.

this would require much more calculations, beyond the scope of this work. This simplified model helps to better understand the impact of Pd and PdO on the surface structure. Results are summarized in Figure 8.

Overall, the results of the DFT study are consistent with other analysis performed on similar Au−Pd systems. The mixing of Pd and Au tends to favor Pd-rich surfaces in oxidative conditions.[50,51]

First, one can see that PdO(101) and Pd_5O_4/Au(111) surfaces are clearly predicted to be favorable under 1 bar of O_2 at 400 °C, relative to the pure metal and bimetallic surfaces. This agrees with our experimental observations. Upon exposure to O_2 at elevated temperatures, segregation and oxidation of Pd are energetically more favorable, as PdO(101) and Pd_5O_4/Au(111) are downhill in energy. It must be noted that all of the sequential surfaces are at lower surface energies than PdML/Au(111), with an enthalpic minimum to aggregate Pd in the surface normal direction to form a "bulklike" PdO structure. This is consistent with our data showing the progressive disappearance of an initial core−shell structure with Pd at the surface. One should also notice that PdO (111) is a less stable termination than PdO(101) according to previously published work.[52]

If PdO is on the surface and becomes reduced upon exposure to H_2 at 400 °C, this can impact the surface of the particles, as we observed in Figure 3c,d. Indeed, the surface energy of PdO(101) surface is lower than the surface energy of metallic Pd(111) surface. Hence, sharp (101) facets are energetically more favorable with PdO than with Pd(111) facets, which could explain the increased surface roughness upon H_2 treatment, which causes sequential reduction of the PdO surface. In fact, the hydride phases during reduction of PdO are metastable and favorable. Thus, H has a transient behavior in the Pd matrix, which could lead to surface roughening. In that case, oxidation of Pd on the surface leads to sharp facets more easily than when the Pd is reduced at elevated temperatures.[50,51,53,54]

DISCUSSION

Faceting of nanoparticles has been documented in previous work.[55−57] In fact, prolonged exposure to elevated temperature should lead nanoparticles to reach an equilibrium shape given by Wulff's theory.[58] For instance, the equilibrium shape of small Au nanoparticles is typically an icosahedron.[59,60] However, the behavior of bimetallic samples can be hard to predict and can be only determined experimentally, as performed in this work. For many $Au_{0.75}Pd_{0.25}$ particles, surface reconstruction was observed at elevated temperatures under O_2 and H_2 associated with minimization of the surface energy.

The partial removal of the core−shell structure upon heating in O_2 was surprising. Indeed, Pd tends to migrate to the surface of particles to form PdO under an oxidative environment. We did observe thin Pd-rich islands on the surface of the particles upon oxidation at 400 °C, but no core−shell configuration was observed, as was the case for a fresh sample. Beam exposure was kept as low as possible to avoid electron irradiation effects during scanning for EDS maps. Hence, we suggest that exposure to elevated temperatures increases the movements of vacancies within the Pd−Au alloy, leading to some Pd atoms

https://doi.org/10.1021/acs.jpcc.2c05929
J. Phys. Chem. C 2022, 126, 18047−18056

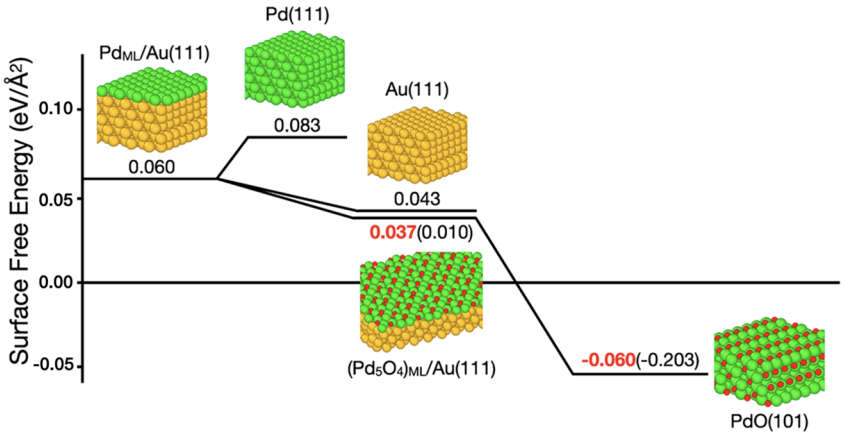

Figure 8. Surface free energy of relevant Pd, Au, PdAu, and O/PdAu surfaces. Values in red denote entropically corrected surface free energies, taking into account the experimental conditions of O_2. The values in parentheses denote the purely enthalpic energies for these structures.

being redistributed inside the core.[61] Thin Pd-rich islands remain on the top of the surface after exposure to O_2 at elevated temperature, which favors surface segregation of Pd (based on DFT results). We speculate that Pd atoms under the surface became redistributed by movement of vacancies due to thermal activation. Thus, two competing forces could explain the redistribution of Pd within $Au_{0.75}Pd_{0.25}$ particles during exposure to O_2 at elevated temperatures. Hence, this study underlines the influence of two mechanisms to explain important changes in the structure of Au−Pd catalysts.

EELS spectra indicate an oxidized state of Pd upon exposure to O_2 at 400 °C for 2 h. The sample is more oxidized than at the beginning of the experiment, although reference spectra of pure PdO show a larger white line.[38] This suggests that the Pd in the nanoparticles is partially oxidized after exposure to O_2 at 400 °C, while some Pd remains metallic. However, it was not possible to locate potential PdO-rich regions within the particles with EELS or EDS. Indeed, the Pd L_3 edge corresponds to a high energy loss, and we needed to collect an average spectrum from 30 to 40 particles to obtain a signal that was not too noisy. (In EELS, the signal-to-noise ratio (SNR) increases at high energy losses.) Additionally, the two SiN windows in the *in situ* cell reduce signal intensity for EELS analysis further. As an example, Pd M edges cannot show shifts in valence states. Finally, the O K edge at 529 eV loss could not be used because the SiN windows contain traces of SiO_2. Hence, the EELS and EDS data for O cannot be used in this study. However, it is reasonable to assume that PdO may be preferentially located on the surface of the particles, as surface Pd is exposed to the O_2. Moreover, previous X-ray absorption spectroscopy (XAS) studies of Au−Pd particles indicate the presence of Pd on the surface upon O_2 treatment at elevated temperatures.[42]

The segregation of Pd to the surface after O_2 treatment is beneficial to expose Pd atoms, which are the main catalyst for many reactions, such as the hydrogenation of hexynes.[7] Increase in activity has been observed in fully reduced particles after exposure to O_2, whereas an exposure to H_2 decreases the activity.[16] Thus, the STEM data are well correlated to catalytic measurements on this system. Increase in activity was also observed after fully reduced particles were exposed to CO, although it was not as high as after an O_2 pretreatment. We speculate that the substantial surface roughening upon exposure to CO creates a unique electronic configuration that is favorable to increase the yield for the hydrogenation of alkynes. Additionally, even though we did not see any segregation of Pd to the surface upon exposure to CO, it is possible that a small and undetected amount of Pd atoms may segregate to the surface and consequently increase the activity of the system.

Finally, the DFT calculations underline the impact of Pd and Pd oxide on the surface energies. Even though this was observed in a minority of particles, the particularly low surface energy of PdO compared to Au−Pd or metallic Pd surface favors the formation of PdO(101) surfaces. This explains the presence of sharp facets which formed upon exposure to oxygen. Hence, we demonstrated the influence of Pd oxide on the morphology of Au−Pd systems, which can impact the surface roughness of the catalyst.

CONCLUSION

We identified dynamic restructuring effects in $Au_{0.75}Pd_{0.25}$ particles upon exposure to O_2, H_2, CO, and CO_2 at elevated temperatures. An increase in temperature leads to sharper facets that minimize surface energy and the loss of an initial core−shell configuration. At 400 °C, most particles did not change when O_2 was replaced with H_2, although in some cases, the surface roughness increased upon exposure to H_2. We suggest that the reduction of PdO to Pd causes subtle facet reconstruction and rougher edges, as the surface energy for a (111) facet of metallic Pd is higher than the surface energy of a PdO(101) facet. Finally, we observed a substantial removal of sharp facets after exposure to CO at room and elevated temperatures. The adsorption of CO seems to modify the stability of facets on $Au_{0.25}Pd_{0.25}$ particles. The adsorbed CO changes the surface energy and induces strain on the surface, leading to a higher sensitivity to the electron beam and the destruction of sharp edges. These dynamical changes play a crucial role in the surface chemistry of $Au_{0.75}Pd_{0.25}$ particles and inform our understanding of differences in catalytic activity after gaseous treatments.

ASSOCIATED CONTENT

Supporting Information

The Supporting Information is available free of charge at https://pubs.acs.org/doi/10.1021/acs.jpcc.2c05929.

Additional *in situ* and *ex situ* STEM images and EDS maps of $Au_{0.75}Pd_{0.25}$ particles; EELS spectra; EDS

https://doi.org/10.1021/acs.jpcc.2c05929
J. Phys. Chem. C 2022, 126, 18047−18056

spectrum; STEM images with indicated facet orientations (PDF)

AUTHOR INFORMATION

Corresponding Author

Eric A. Stach − *Department of Materials Science and Engineering, University of Pennsylvania, Philadelphia, Pennsylvania 19104, United States;* orcid.org/0000-0002-3366-2153; Email: stach@seas.upenn.edu

Authors

Alexandre C. Foucher − *Department of Materials Science and Engineering, University of Pennsylvania, Philadelphia, Pennsylvania 19104, United States;* orcid.org/0000-0001-5042-4002

Cameron J. Owen − *Department of Chemistry and Chemical Biology, Harvard University, Cambridge, Massachusetts 02138, United States;* orcid.org/0000-0002-2543-7415

Tanya Shirman − *John A. Paulson School of Engineering and Applied Sciences, Harvard University, Cambridge, Massachusetts 02138, United States*

Joanna Aizenberg − *Department of Chemistry and Chemical Biology and John A. Paulson School of Engineering and Applied Sciences, Harvard University, Cambridge, Massachusetts 02138, United States;* orcid.org/0000-0002-2343-8705

Boris Kozinsky − *John A. Paulson School of Engineering and Applied Sciences, Harvard University, Cambridge, Massachusetts 02138, United States; Robert Bosch Research and Technology Center, Cambridge, Massachusetts 02139, United States;* orcid.org/0000-0002-0638-539X

Complete contact information is available at: https://pubs.acs.org/10.1021/acs.jpcc.2c05929

Notes

The authors declare the following competing financial interest(s): One of the authors (E.A.S.) has an equity interest in Hummingbird Scientific.

ACKNOWLEDGMENTS

This work was supported as part of the Integrated Mesoscale Architectures for Sustainable Catalysis (IMASC), an Energy Frontier Research Center funded by the U.S. Department of Energy, Office of Science, Basic Energy Sciences, under Award #DE-SC0012573. C.J.O. was supported by the National Science Foundation Graduate Research Fellowship Program under Grant DGE1745303. C.J.O. used computing resources provided by the Harvard University FAS Division of Science Research Computing Group. Experiments were also performed at the Singh Center for Nanotechnology at the University of Pennsylvania, supported by the National Science Foundation (NSF) National Nanotechnology Coordinated Infrastructure Program Grant NNCI-1542153. Additional support for the Nanoscale Characterization Facility at the Singh Center has been provided by the Laboratory for Research on the Structure of Matter (MRSEC) supported by the National Science Foundation (DMR-1720530). Nanoparticle synthesis and preparation were supported as part of the Catalysis Center for Energy Innovation, an Energy Frontier Research Center funded by the U.S. Department of Energy, Office of Science, Office of Basic Energy Sciences, under Award DE-SC0001004. The authors thank Pr. Frances Ross at the Massachusetts Institute of Technology for access to the environmental TEM (Hitachi HF5000) to perform low-pressure *in situ* analysis, shown in Figure S10.

REFERENCES

(1) Li, Y.; Yu, Y.; Wang, J. G.; Song, J.; Li, Q.; Dong, M.; Liu, C. J. CO Oxidation over Graphene Supported Palladium Catalyst. *Appl. Catal. B Environ.* **2012**, *125*, 189−196.

(2) Peterson, E. J.; DeLaRiva, A. T.; Lin, S.; Johnson, R. S.; Guo, H.; Miller, J. T.; Kwak, J. H.; Peden, C. H. F.; Kiefer, B.; Allard, L. F.; et al. Low-Temperature Carbon Monoxide Oxidation Catalysed by Regenerable Atomically Dispersed Palladium on Alumina. *Nat. Commun.* **2014**, *5*, 1−11.

(3) Patel, V. K.; Sharma, S. Effect of Oxide Supports on Palladium Based Catalysts for NO Reduction by H_2-SCR. *Catal. Today* **2021**, *375*, 591−600.

(4) Teschner, D.; Vass, E.; Hävecker, M.; Zafeiratos, S.; Schnörch, P.; Sauer, H.; Knop-Gericke, A.; Schlögl, R.; Chamam, M.; Wootsch, A.; et al. Alkyne Hydrogenation over Pd Catalysts: A New Paradigm. *J. Catal.* **2006**, *242*, 26−37.

(5) Lindlar, H. Ein Neuer Katalysator Für Selektive Hydrierungen. *Helv. Chim. Acta* **1952**, *35*, 446−450.

(6) Vilé, G.; Albani, D.; Nachtegaal, M.; Chen, Z.; Dontsova, D.; Antonietti, M.; López, N.; Pérez-Ramírez, J. A Stable Single-Site Palladium Catalyst for Hydrogenations. *Angew. Chemie - Int. Ed.* **2015**, *54*, 11265−11269.

(7) Luneau, M.; Shirman, T.; Foucher, A. C.; Duanmu, K.; Verbart, D. M. A.; Sautet, P.; Stach, E. A.; Aizenberg, J.; Madix, R. J.; Friend, C. M. Achieving High Selectivity for Alkyne Hydrogenation at High Conversions with Compositionally Optimized PdAu Nanoparticle Catalysts in Raspberry Colloid-Templated SiO_2. *ACS Catal.* **2020**, *10*, 441−450.

(8) Nutt, M. O.; Heck, K. N.; Alvarez, P.; Wong, M. S. Improved Pd-on-Au Bimetallic Nanoparticle Catalysts for Aqueous-Phase Trichloroethene Hydrodechlorination. *Appl. Catal. B Environ.* **2006**, *69*, 115−125.

(9) Liu, T.; Zhou, H.; Han, B.; Gu, Y.; Li, S.; Zheng, J.; Zhong, X.; Zhuang, G. L.; Wang, J. G. Enhanced Selectivity of Phenol Hydrogenation in Low-Pressure CO_2 over Supported Pd Catalysts. *ACS Sustain. Chem. Eng.* **2017**, *5*, 11628−11636.

(10) Sun, Y.; Dai, S. High-Entropy Materials for Catalysis: A New Frontier. *Sci. Adv.* **2021**, *7*, eabg1600.

(11) Tang, W.; Zhang, L.; Henkelman, G. Catalytic Activity of Pd/Cu Random Alloy Nanoparticles for Oxygen Reduction. *J. Phys. Chem. Lett.* **2011**, *2*, 1328−1331.

(12) El Kolli, N.; Delannoy, L.; Louis, C. Bimetallic Au−Pd Catalysts for Selective Hydrogenation of Butadiene: Influence of the Preparation Method on Catalytic Properties. *J. Catal.* **2013**, *297*, 79−92.

(13) van der Hoeven, J. E. S.; Jelic, J.; Olthof, L. A.; Totarella, G.; van Dijk-Moes, R. J. A.; Krafft, J.-M.; Louis, C.; Studt, F.; van Blaaderen, A.; de Jongh, P. E. Unlocking Synergy in Bimetallic Catalysts by Core−Shell Design. *Nat. Mater.* **2021**, *20*, 1216−1220.

(14) van der Hoeven, J. E. S.; Ngan, H. T.; Taylor, A.; Eagan, N. M.; Aizenberg, J.; Sautet, P.; Madix, R. J.; Friend, C. M. Entropic Control of HD Exchange Rates over Dilute Pd-in-Au Alloy Nanoparticle Catalysts. *ACS Catal.* **2021**, *11*, 6971−6981.

(15) Kortlever, R.; Peters, I.; Balemans, C.; Kas, R.; Kwon, Y.; Mul, G.; Koper, M. T. M. Palladium−Gold Catalyst for the Electrochemical Reduction of CO_2 to C1−C5 Hydrocarbons. *Chem. Commun.* **2016**, *52*, 10229−10232.

(16) Luneau, M.; Guan, E.; Chen, W.; Foucher, A. C.; Marcella, N.; Shirman, T.; Verbart, D. M. A.; Aizenberg, J.; Aizenberg, M.; Stach, E. A.; et al. Enhancing Catalytic Performance of Dilute Metal Alloy Nanomaterials. *Commun. Chem.* **2020**, *3*, 1−9.

(17) Guan, E.; Foucher, A. C.; Marcella, N.; Shirman, T.; Luneau, M.; Head, A. R.; Verbart, D. M. A.; Aizenberg, J.; Friend, C. M.; Stacchiola, D.; et al. New Role of Pd Hydride as a Sensor of Surface

Pd Distributions in Pd−Au Catalysts. *ChemCatChem* **2020**, *12*, 717−721.
(18) Zhang, Z.; Wang, S.-S.; Song, R.; Cao, T.; Luo, L.; Chen, X.; Gao, Y.; Lu, J.; Li, W.-X.; Huang, W. The Most Active Cu Facet for Low-Temperature Water Gas Shift Reaction. *Nat. Commun.* **2017**, *8*, 1−10.
(19) Pal, J.; Pal, T. Faceted Metal and Metal Oxide Nanoparticles: Design, Fabrication and Catalysis. *Nanoscale* **2015**, *7*, 14159−14190.
(20) De Gregorio, G. L.; Burdyny, T.; Loiudice, A.; Iyengar, P.; Smith, W. A.; Buonsanti, R. Facet-Dependent Selectivity of Cu Catalysts in Electrochemical CO_2 Reduction at Commercially Viable Current Densities. *ACS Catal.* **2020**, *10*, 4854−4862.
(21) Yuan, W.; Zhu, B.; Fang, K.; Li, X.-Y.; Hansen, T. W.; Ou, Y.; Yang, H.; Wagner, J. B.; Gao, Y.; Wang, Y.; Zhang, Z. In situ Manipulation of the Active Au-TiO_2 interface with Atomic Precision during CO Oxidation. *Science* **2021**, *371* (6528), 517.
(22) Yoshida, H.; Kuwauchi, Y.; Jinschek, J. R.; Sun, K.; Tanaka, S.; Kohyama, M.; Shimada, S.; Haruta, M.; Takeda, S. Visualizing Gas Molecules Interacting with Supported Nanoparticulate Catalysts at Reaction Conditions. *Science* **2012**, *335*, 317−319.
(23) Song, B.; Yang, T. T.; Yuan, Y.; Sharifi-Asl, S.; Cheng, M.; Saidi, W. A.; Liu, Y.; Shahbazian-Yassar, R. Revealing Sintering Kinetics of MoS_2-Supported Metal Nanocatalysts in Atmospheric Gas Environments via Operando Transmission Electron Microscopy. *ACS Nano* **2020**, *14*, 4074−4086.
(24) Kang, Y.; Pyo, J. B.; Ye, X.; Diaz, R. E.; Gordon, T. R.; Stach, E. A.; Murray, C. B. Shape-Controlled Synthesis of Pt Nanocrystals: The Role of Metal Carbonyls. *ACS Nano* **2013**, *7*, 645−653.
(25) Wang, R.; He, H.; Wang, J.; Liu, L.; Dai, H. Shape-Regulation: An Effective Way to Control CO Oxidation Activity over Noble Metal Catalysts. *Catal. Today* **2013**, *201*, 68−78.
(26) Mejía-Rosales, S. J.; Fernández-Navarro, C.; Pérez-Tijerina, E.; Blom, D. A.; Allard, L. F.; José-Yacamán, M. On the Structure of Au/Pd Bimetallic Nanoparticles. *J. Phys. Chem. C* **2007**, *111*, 1256−1260.
(27) Ding, Y.; Fan, F.; Tian, Z.; Wang, Z. L. Atomic Structure of Au-Pd Bimetallic Alloyed Nanoparticles. *J. Am. Chem. Soc.* **2010**, *132*, 12480−12486.
(28) Luneau, M.; Shirman, T.; Filie, A.; Timoshenko, J.; Chen, W.; Trimpalis, A.; Flytzani-Stephanopoulos, M.; Kaxiras, E.; Frenkel, A. I.; Aizenberg, J.; et al. Dilute Pd/Au Alloy Nanoparticles Embedded in Colloid-Templated Porous SiO_2: Stable Au-Based Oxidation Catalysts. *Chem. Mater.* **2019**, *31*, 5759−5768.
(29) Xin, H. L.; Niu, K.; Alsem, D. H.; Zheng, H. In situ TEM Study of Catalytic Nanoparticle Reactions in Atmospheric Pressure Gas Environment. *Microsc. Microanal.* **2013**, *19*, 1558−1568.
(30) Zhao, S.; Li, Y.; Stavitski, E.; Tappero, R.; Crowley, S.; Castaldi, M. J.; Zakharov, D. N.; Nuzzo, R. G.; Frenkel, A. I.; Stach, E. A. Operando Characterization of Catalysts through Use of a Portable Microreactor. *ChemCatChem* **2015**, *7*, 3683−3691.
(31) Kresse, G. Ab Initio Molecular Dynamics for Liquid Metals. *J. Non. Cryst. Solids* **1995**, *192*−*193*, 222−229.
(32) Perdew, J. P.; Burke, K.; Ernzerhof, M. Generalized Gradient Approximation Made Simple. *Phys. Rev. Lett.* **1996**, *77*, 3865.
(33) Blöchl, P. E. Projector Augmented-Wave Method. *Phys. Rev. B* **1994**, *50*, 17953.
(34) Marcella, N.; Lim, J. S.; Płonka, A. M.; Yan, G.; Owen, C. J.; van der Hoeven, J. E. S.; Foucher, A. C.; Ngan, H. T.; Torrisi, S. B.; Marinkovic, N. S.; et al. Decoding Reactive Structures in Dilute Alloy Catalysts. *Nat. Commun.* **2022**, *13*, 1−9.
(35) Hjorth Larsen, A.; JØrgen Mortensen, J.; Blomqvist, J.; Castelli, I. E.; Christensen, R.; Dułak, M.; Friis, J.; Groves, M. N.; Hammer, B.; Hargus, C.; et al. The Atomic Simulation Environment-a Python Library for Working with Atoms. *J. Phys.: Condens. Matter* **2017**, *29*, 273002.
(36) Krivanek, O. L.; Chisholm, M. F.; Nicolosi, V.; Pennycook, T. J.; Corbin, G. J.; Dellby, N.; Murfitt, M. F.; Own, C. S.; Szilagyi, Z. S.; Oxley, M. P.; et al. Atom-by-Atom Structural and Chemical Analysis by Annular Dark-Field Electron Microscopy. *Nat.* **2010**, *464*, 571−574.
(37) Egerton, R. F. *Electron Energy-Loss Spectroscopy in the Electron Microscopy*; Springer: 2011.
(38) PalladiumlEELS.info https://eels.info/atlas/palladium (accessed 2022-03-08).
(39) Marks, L. D.; Marks, L. D. Surface Structure and Energetics of Multiply Twinned Particles. *Philos. Mag. A Phys. Condens. Matter, Struct. Defects Mech. Prop.* **1984**, *49*, 81−93.
(40) Bonifacio, C. S.; Carenco, S.; Wu, C. H.; House, S. D.; Bluhm, H.; Yang, J. C. Thermal Stability of Core-Shell Nanoparticles: A Combined *in situ* Study by XPS and TEM. *Chem. Mater.* **2015**, *27*, 6960−6968.
(41) Schnedlitz, M.; Lasserus, M.; Meyer, R.; Knez, D.; Hofer, F.; Ernst, W. E.; Hauser, A. W. Stability of Core-Shell Nanoparticles for Catalysis at Elevated Temperatures: Structural Inversion in the Ni-Au System Observed at Atomic Resolution. *Chem. Mater.* **2018**, *30*, 1113−1120.
(42) Boubnov, A.; Timoshenko, J.; Wrasman, C. J.; Hoffman, A. S.; Cargnello, M.; Frenkel, A. I.; Bare, S. R. Insight into Restructuring of Pd-Au nanoparticles using EXAFS. *Radiat. Phys. Chem.* **2020**, *175*, 108304.
(43) Solymosi, F. The Bonding, Structure and Reactions of CO_2 Adsorbed on Clean and Promoted Metal Surfaces. *J. Mol. Catal.* **1991**, *65*, 337−358.
(44) Pachecka, M.; Sturm, J. M.; Lee, C. J.; Bijkerk, F. Adsorption and Dissociation of CO_2 on Ru(0001). *J. Phys. Chem. C. Nanomater. Interfaces* **2017**, *121*, 6729.
(45) Martin, N. M.; Van Den Bossche, M.; Grönbeck, H.; Hakanoglu, C.; Zhang, F.; Li, T.; Gustafson, J.; Weaver, J. F.; Lundgren, E. CO Adsorption on Clean and Oxidized Pd(111). *J. Phys. Chem. C* **2014**, *118*, 1118−1128.
(46) Tao, F. F.; Nguyen, L.; Zhang, S.; Li, Y.; Tang, Y.; Zhang, L.; Frenkel, A. I.; Xia, Y.; Salmeron, M. Formation of Second-Generation Nanoclusters on Metal Nanoparticles Driven by Reactant Gases. *Nano Lett.* **2016**, *16*, 5001−5009.
(47) Kolesnikov, A. L.; Budkov, Y. A.; Gor, G. Y. Models of Adsorption-Induced Deformation: Ordered Materials and Beyond. *J. Phys.: Condens. Matter* **2021**, *34*, 063002.
(48) Chen, B.; Zhang, C. H.; Jin, Y. Tensile Strain Induced Surface Reactions for Co-Adsorption of H_2O and OH− on Vacancy Al (111) Surface. *Vacuum* **2021**, *192*, 110459.
(49) Fujita, T.; Guan, P.; Mckenna, K.; Lang, X.; Hirata, A.; Zhang, L.; Tokunaga, T.; Arai, S.; Yamamoto, Y.; Tanaka, N. Atomic Origins of the High Catalytic Activity of Nanoporous Gold. *Nat. Mater.* **2012**, *11*, 775.
(50) Todorova, D.-P. M. Oxidation of Palladium Surfaces. Doctoral Thesis, Technical University Berlin, Berlin, 2004.
(51) Sterrer, M.; Freund, H-J. Properties of Oxide Surfaces. In *Surfaces and Interface Science: Properties of Composite Surfaces: Alloys, Compounds, Semiconductors*, 1st ed.;Wandelt, K., Ed.; Wiley-VCH Verlag GmbH & Co: Weinheim, 2014.
(52) Rogal, J.; Reuter, K.; Scheffler, M. Thermodynamic Stability of PdO Surfaces. *Phys. Rev. B* **2004**, *69*, 075421.
(53) Long, R.; Mao, K.; Ye, X.; Yan, W.; Huang, Y.; Wang, J.; Fu, Y.; Wang, X.; Wu, X.; Xie, Yi.; et al. Surface Facet of Palladium Nanocrystals: A Key Parameter to the Activation of Molecular Oxygen for Organic Catalysis and Cancer Treatment. *J. Am. Chem. Soc.* **2013**, *135*, 3200−3207.
(54) Seriani, N.; Harl, J.; Mittendorfer, F.; Kresse, G. A First-Principles Study of Bulk Oxide Formation on Pd(100). *J. Chem. Phys.* **2009**, *131*, 054701.
(55) Chi, M.; Wang, C.; Lei, Y.; Wang, G.; Li, D.; More, K. L.; Lupini, A.; Allard, L. F.; Markovic, N. M.; Stamenkovic, V. R. Surface Faceting and Elemental Diffusion Behaviour at Atomic Scale for Alloy Nanoparticles during *in situ* Annealing. *Nat. Commun.* **2015**, *6*, 1−9.
(56) Ermanoski, I.; Pelhos, K.; Chen, W.; Quinton, J. S.; Madey, T. E. Oxygen-Induced Nano-Faceting of Ir(210). *Surf. Sci.* **2004**, *549*, 1−23.

https://doi.org/10.1021/acs.jpcc.2c05929
J. Phys. Chem. C 2022, 126, 18047−18056

(57) Kaghazchi, P.; Simeone, F. C.; Soliman, K. A.; Kibler, L. A.; Jacob, T. Bridging the Gap between Nanoparticles and Single Crystal Surfaces. *Faraday Discuss.* **2009**, *140*, 69−80.
(58) Wulff, G. XXV. Zur Frage Der Geschwindigkeit Des Wachsthums Und Der Auflösung Der Krystallflächen. *Zeitschrift für Krist. - Cryst. Mater.* **1901**, *34*, 449−530.
(59) Zhang, C.; Zhang, J.; Han, B.; Zhao, Y.; Li, W. Synthesis of Icosahedral Gold Particles by a Simple and Mild Route. *Green Chem.* **2008**, *10*, 1094−1098.
(60) Liu, M.; Guyot-Sionnest, P. Mechanism of Silver(I)-Assisted Growth of Gold Nanorods and Bipyramids. *J. Phys. Chem. B* **2005**, *109*, 22192−22200.
(61) Liu, Y.; Wu, H.; Wang, Y.; Li, K.; Yin, S.; Dahn, J. R. Impact of Shell Composition, Thickness and Heating Temperature on the Performance of Nickel-Rich Cobalt-Free Core-Shell Materials. *J. Electrochem. Soc.* **2020**, *167*, 160556.

https://doi.org/10.1021/acs.jpcc.2c05929
J. Phys. Chem. C 2022, 126, 18047−18056